Dynamic wave-packet scattering in autoionizing two-electron atoms

R. van Leeuwen, M. L. Bajema, and R. R. Jones
Department of Physics, University of Virginia, Charlottesville, Virginia 22901
(Received 7 June 1999; published 13 January 2000)

We have studied the propagation of an autoionizing radial Rydberg wave packet in barium. The wave packet is formed when a short laser pulse directly excites two quasibound low-n $5d_{5/2}nd$ Rydberg states that are embedded in the continuum above the first ionization threshold. This two-state autoionizing radial wave packet interacts strongly with high-n' Rydberg states associated with the adjacent $5d_{3/2}n'd$ series. Time-dependent electron-electron scattering leads to the formation of three distinct bound radial wave packets that oscillate with very different Kepler periods and periodically decay through autoionization. Experimentally, we have probed the temporal oscillations between the different wave packets with a second, time-delayed, laser pulse using bound-state interferometry. Theoretically, we use three-channel quantum-defect theory to construct and propagate the multiconfigurational wave packet to view its spatial distribution as a function of time.

PACS number(s): 32.80.Dz, 32.80.Rm

I. INTRODUCTION

The widespread availability of short pulsed lasers with spectral bandwidths larger than energy-level spacings in Rydberg atoms has led to extensive studies of the dynamic behavior of Rydberg wave packets. Initially much of the experimental research focused on atoms in single configurations [1], but more recently multiconfigurational two-electron systems have received theoretical [2,3] and experimental [4–8] attention as well. When coherently excited by a short pulse, these systems can exhibit temporal oscillations between different configurations as a result of dynamic electron-electron scattering [2]. This time-dependent configuration interaction is analogous to the more complicated process of population transfer between different rotational and vibrational modes in molecules. Hence, two-electron atoms provide relatively simple systems to investigate processes relevant to the quantum control of chemical reactions [9].

Previous experiments have investigated the role of time-dependent configuration interaction in systems with varying degrees of complexity. The first time-domain experiments examined the interaction of a single bound doubly excited valence state with a singly excited Rydberg series [4]. Direct excitation of pure Rydberg or pure valence modes resulted in a clear oscillation of wave-packet character between these two nonstationary configurations. Population beating between degenerate bound modes has also been observed in the case where two configurationally mixed autoionizing states are simultaneously excited [5]. In addition, optical control over the autoionization rate [8] and branching ratio for decay in these systems has been demonstrated [7]. More recently, the production of a shock-wave packet [10] via the rapid coupling of a stationary Rydberg state to the continuum in a sudden isolated core excitation (ICE) [11] has been studied [6]. All these experiments clearly demonstrate that scattering between the Rydberg and ''core'' electron results in dynamic manipulation of the Rydberg electron probability distribution.

Here we present the results of what to our knowledge is the first experimental investigation of time-dependent configuration interaction between two configurationally mixed *series*, not simply isolated resonances, embedded in a common continuum. In the experiment, a 100-fs laser pulse produces an autoionizing wave packet by photoexciting barium atoms from a tightly bound eigenstate into the structured continuum approximately 0.6 eV above the $Ba^+(6s)$ ionization threshold. Immediately following the excitation the wave packet can be described as a coherent superposition of two bound $5d_{5/2}nd$ Rydberg eigenstates. In the absence of any other bound channels, the Rydberg probability distribution would undergo radial oscillations with 160-fs Kepler period. However, each time the wave packet nears the $Ba^+(5d_{5/2})$ core, there is a significant probability for scattering between the Rydberg and ''core'' electrons. These scattering events lead to deexcitation of the $5d_{5/2}$ core to $5d_{3/2}$ or $6s_{1/2}$ ionic levels with an associated excitation of the Rydberg electron to higher-lying bound $n'd$ states or continuum ϵs levels, respectively. Scattering into the $5d_{3/2}n'd$ channel results in the creation of two additional radial wave packets, with larger spatial extent and longer Kepler periods. At any given time the three spatially distinct Rydberg wave packets and their associated core configurations are entangled in the two-electron wave function. We probe the complicated evolution of this two-electron wave packet using a second laser pulse to form a bound-state interferometer [12]. Our experimental results are interpreted theoretically by propagating the two-electron wave function in the time domain. The wave functions are calculated using standard multichannel quantum-defect theory (MQDT) [13,14].

This paper is organized as follows. In Sec. II we describe the details of the multiconfigurational two-electron system, the experimental method, and the experimental results. In Sec. III we derive analytical expressions for the bound-state interferogram, as well as the spatial distribution and temporal evolution of the autoionizing wave packet in terms of MQDT parameters. In Sec. IV we show that the experimental data can be adequately described using two bound and one continuum channel to calculate the dynamics of the wave packet. The results of our numerical simulation are discussed in Sec. V and we summarize our findings in Sec. VI.

II. EXPERIMENT

The multiconfigurational wave packets are produced by short-pulse photoexcitation of barium atoms from an inter-

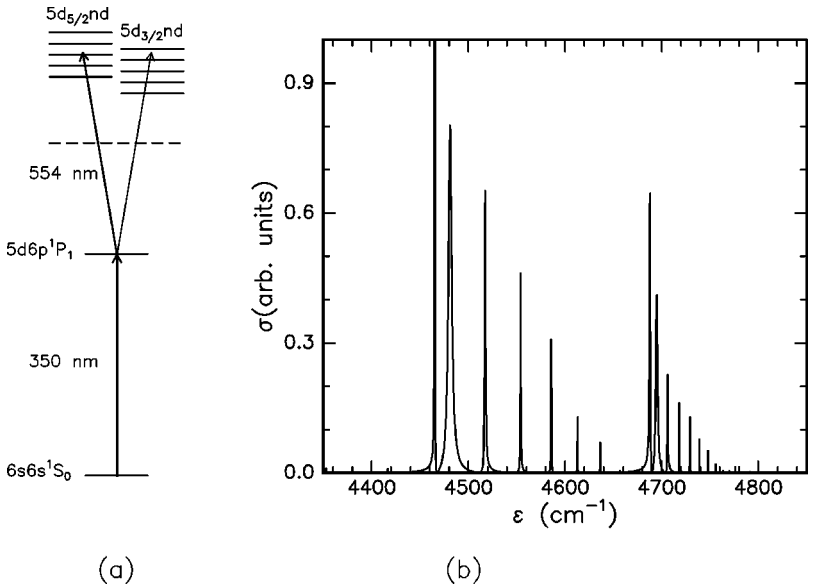

FIG. 1. Barium excitation. (a) Two-step resonant laser excitation scheme. (b) Calculated cross section for excitation from the intermediate $5d6p\,^1P_1$ state by a short laser pulse with a frequency spectrum identical to that used in the experiment.

mediate $5d6p\ ^1P_1$ state to an energy range above the first $Ba^+(6s_{1/2})$ ionization limit but just below the $Ba^+(5d_j)$ ionization limits [see Fig. 1(a)]. In principle, eight bound and three continuum $J=0,2$ channels are optically accessible in the experiment. However, in practice direct excitation is limited to the three bound $J=0$ channels. Specifically, we excite $5d_jnd_jJ=0$ $(j=3/2,5/2)$ bound configurations embedded in the $6s_{1/2}\epsilon s_{1/2}J=0$ continuum. The absence of the $5dns$ and $5dnd$ $J=2$ channels is presumably due to small radial and angular matrix elements between the intermediate $5d6p$ state and the final channels, respectively. Figure 1(b) shows the theoretical cross section for the excitation over the energy range of interest in the experiment (see Sec. III). The spectrum is dominated by two strong $5d_{5/2}nd_{5/2}$ transitions with Rydberg electron principal quantum numbers $n=12$ and $n=13$. Although angular selection rules do not favor direct excitation of the nearby $5d_{3/2}n'd_{3/2}$ levels, peaks in the cross section appear at these resonances due to configurational mixing with the $5d_{5/2}nd_{5/2}$ channel. There is essentially zero direct continuum excitation from the $5d6p$ intermediate state, and the autoionization linewidth of the $5dnd$ states is determined by the coupling strength to the $6s\epsilon s$ continuum.

If we consider the laser excitation in the time domain, a wave packet localized in the bound $5d_{5/2}$ channel is created at time $t=0$. However, after some time, coherent scattering into the $5d_{3/2}$ bound channel or the $6s_{1/2}$ continuum channel occurs [4,5,7]. Population can also be transferred from the $5d_{3/2}$ channel back into the $5d_{5/2}$ configuration, but eventually all the bound population is depleted due to scattering into the continuum [5,7]. We monitor the total number of atoms excited to autoinizing states by detecting the $Ba^+(6s_{1/2})$ ions or low-energy (0.5 eV) electrons produced via autoionization.

The laser pulse used to create the wave packet has a 100-fs duration, a center wavelength of 554 nm, a bandwidth of 180 cm^{-1}, and is generated in an optical parametric amplifier (OPA). The OPA is pumped by half the output of a 2-W Ti:sapphire regenerative amplifier operating at 800 nm with a 1-kHz repetition rate. Approximately 30 mW of 554-nm laser light is produced by sum frequency mixing the 1.80-μm idler beam from the OPA with the residual 800-nm pump beam in a BBO crystal.

A second OPA, pumped by the other half of the output of the regenerative amplifier, is used to populate the intermediate $5d6p\ ^1P_1$ launch state from the $6s6s\ ^1S_0$ ground state. The 1.4-μm signal beam from this OPA is converted to 1 mW of 350-nm laser light by fourth harmonic generation in two stages. A 4-cm-long KDP crystal is used to double the frequency of the 700-nm doubled signal beam. Due to phase matching in the long crystal, the bandwidth of the 350-nm pulse is only 10 cm^{-1}, enhancing the population transfer to the spectrally narrow $5d6p\ ^1P_1$ state.

The two laser beams are overlapped and focused by a 50-cm focal-length lens into a beam of ground-state barium atoms that effuse from a resistively heated oven. The interaction region is located between two grounded capacitor plates. Approximately 50 ns after the laser excitation, a 100-V pulse applied to one of the plates pushes the Ba^+ ions resulting from autoionization into a microchannel plate detector.

The evolution of the autoionizing wave packet is probed by exposing the barium atoms to a second identical, phase-coherent laser pulse [12]. After some time delay τ the second pulse creates a second wave packet within each atom. Depending on the phase difference between the two laser pulses, constructive or destructive interference occurs between the two wave packets, altering the net ion yield from the two-pulse excitation. The magnitude of the variation in the autoionization yield as a function of the relative pulse delay is a measure of how much the wave packet at time τ resembles its initial spatial distribution and core configuration. In this experiment, the interference signal reflects how much of the first wave packet remains in the $5d_{5/2}$ channel *and* is close to the Ba^+ core at $t=\tau$.

The phase coherent pulse pair is produced by sending the 554-nm beam through a Michelson interferometer. The time delay between the two pulses is scanned by varying the op-

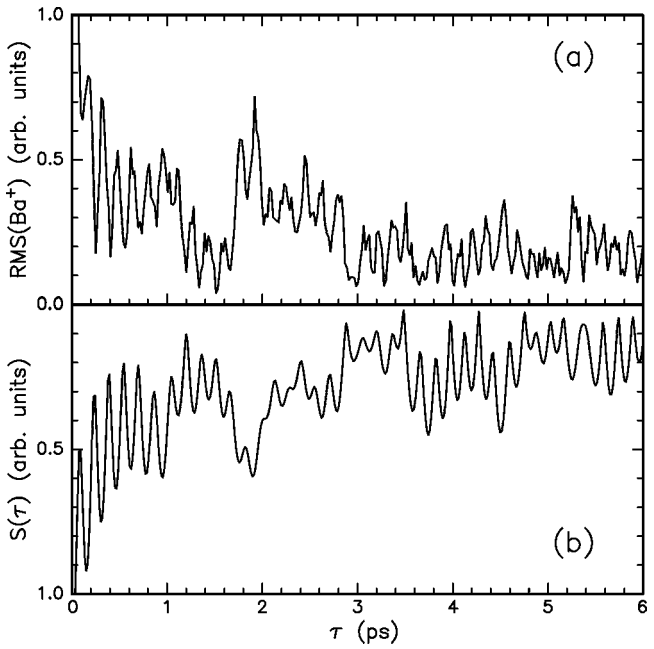

FIG. 2. (a) Experimental rms ion signal as a function of the relative delay between the two phase-coherent laser pulses. (b) Calculated bound-state rms interferogram obtained from the experimental MQDT parameters using Eq. (9). Note that the *y* scale in (b) is reversed relative to that in (a) for a mirror image effect.

tical path length of one arm of the interferometer using a piezoelectric controlled translation stage. The variation in the Ba^+ signal is monitored as a function of the time delay between the two laser pulses. Approximately 10 data points per interference cycle are recorded and stored on a personal computer. The time-delay scans are calibrated by simultaneously monitoring the intensity fringes in a continuous-wave HeNe laser beam that passes through the same interferometer. This calibration allows us to retrieve the frequency spectrum of the short laser pulse using the electric-field autocorrelation that is obtained by monitoring the 554-nm transmission through the interferometer. The short-pulse spectrum is simply the Fourier transform of the field autocorrelation.

The magnitude of the variation in the ion signal is obtained by taking the root-mean-square (rms) of the autoionization yield over ten optical frequency interference oscillations. Figure 2(a) shows the rms Ba^+ signal as a function of the time delay τ. The 160-fs modulation in the rms signal is due to the radial motion of the wave packet localized in the $5d_{5/2}$ channel as it oscillates back and forth with a 160-fs Kepler period. In the absence of bound channel interaction we would simply observe this beating with an exponentially decreasing amplitude. However, each time the Rydberg electron passes the core, some electron amplitude scatters into the $5d_{3/2}$ channel, forming two additional Rydberg wave packets that orbit the core with distinctly different Kepler periods of 0.95 and 2.5 ps, respectively. Since electron-electron scattering is restricted to a small volume around the ion core, probability launched as a $5d_{3/2}$ wave packet requires at least 1 ps before it can return to the core and couple back into the $5d_{5/2}$ channel. In spite of rapid autoionization out of the $5d_{5/2}$ configuration, the radial oscillations of the $5d_{5/2}$ wave packet remain prominent for many picoseconds due to ''storing'' or ''shelving'' of bound-state amplitude in the longer lived $5d_{3/2}$ channel. This and other features in Fig. 2(a) will be discussed in more detail in Sec. IV.

III. ANALYTICAL FRAMEWORK

Over the range of energies of interest in the current experiment, the even-parity $J=0$, two-electron eigenstates of the barium atom are described by a total wave function ψ^ϵ that is a linear combination of two bound channel wave functions, $\phi_1^\epsilon = 5d_{5/2}\nu_1^\epsilon d_{5/2} J=0$, and $\phi_2^\epsilon = 5d_{3/2}\nu_2^\epsilon d_{3/2} J=0$ and one continuum channel wave function $\phi_3^\epsilon = 6s_{1/2}\epsilon s_{1/2} J=0$:

$$\psi^\epsilon(\mathbf{r}) = A_1^\epsilon \phi_1^\epsilon(\mathbf{r}) + A_2^\epsilon \phi_2^\epsilon(\mathbf{r}) + A_3^\epsilon \phi_3^\epsilon(\mathbf{r}), \tag{1}$$

where A_j^ϵ are the energy-dependent spectral amplitudes and ϵ is the state energy relative to the $Ba^+(6s_{1/2})$ ionization threshold. The effective principal quantum numbers of the bound channels ν_j^ϵ are related to the energy ϵ through the Rydberg formula $\epsilon = I_j - R/\nu_j^{\epsilon 2}$, where R is the mass-corrected Rydberg constant $R = 109\,736.87\ \mathrm{cm}^{-1}$ and I_j are the ionization limits for the bound channels, i.e., the $Ba^+(5d_{5/2,3/2})$ levels, $I_1 = 5674.82\ \mathrm{cm}^{-1}$, and $I_2 = 4873.85\ \mathrm{cm}^{-1}$, respectively [15]. The channel wave functions can be expressed as

$$\phi_j^\epsilon(\mathbf{r}) = \frac{u_j^\epsilon(r)}{r}\chi_j(\mathbf{r}), \tag{2}$$

where $u_j^\epsilon(r)/r$ are the energy normalized radial wave functions of the least bound (or ''outer'') electron, and $\chi_j(\mathbf{r})$ is a product of the angular part of the outer electron's wave function and the core electron's wave function. The radial wave functions are, if taken to be Coulombic, linear combinations of regular and irregular Coulomb wave functions. Alternatively they can be calculated numerically by integrating the one-electron Schrödinger equation in the appropriate pseudopotential.

Our short laser pulse excites a coherent superposition of a continuum of eigenstates. The resulting wave packet $\Psi(\mathbf{r},t)$ is therefore given by a continuous sum,

$$\Psi(\mathbf{r},t) = \int_{-\infty}^{+\infty} c^\epsilon(t)\psi^\epsilon(\mathbf{r}) e^{-i\epsilon t}\, d\epsilon, \tag{3}$$

where the $c^\epsilon(t)$ depend on the excitation process. The probability for finding the wave packet in channel j at a particular radial position at a specific time is obtained by integrating $|\Psi(\mathbf{r},t)|^2$ over all angles,

$$P_j(r,t) = \left| \int_{-\infty}^{+\infty} c^\epsilon(t) A_j^\epsilon u_j^\epsilon(r) e^{-i\epsilon t} d\epsilon \right|^2. \tag{4}$$

Here we used the fact that the wave functions $\phi_j^\epsilon(\mathbf{r})$ for different channels are orthogonal due to different core configurations $\chi_j(\mathbf{r})$. The probability that the wave packet is, at

some time t, localized in channel j is obtained by integrating Eq. (4) with respect to the radial position,

$$P_j(t)=\int_0^\infty P_j(r,t)dr. \tag{5}$$

At any given time the electron must be in one of the three available channels so that $\Sigma_j P_j(t)=1$.

To calculate the probabilities given by Eqs. (4) and (5) we need to derive an expression for the spectral amplitudes A_j^ϵ and coefficients $c^\epsilon(t)$. This can be done using the phase-shifted R-matrix formulation of MQDT as developed by Cooke and Cromer [14]. In this formalism, shifted principal quantum numbers are defined as $\nu_j'^\epsilon=\nu_j^\epsilon+\delta_j$, where δ_j are single-channel quantum defects. The δ_i can be viewed as the quantum defects of the bound channels in the absence of interseries interactions. The spectral amplitudes are obtained by solving the MQDT equation

$$\begin{pmatrix} \tan\pi\nu_1'^\epsilon & R'_{12} & R'_{13} \\ R'_{12} & \tan\pi\nu_2'^\epsilon & R'_{23} \\ R'_{13} & R'_{23} & -\tan\tau^\epsilon \end{pmatrix} \begin{pmatrix} A_1^\epsilon\cos\pi\nu_1'^\epsilon \\ A_2^\epsilon\cos\pi\nu_2'^\epsilon \\ A_3^\epsilon\cos\tau^\epsilon \end{pmatrix}=0, \tag{6}$$

where R'_{ij} are the phase-shifted parameters describing the channel interactions and τ^ϵ is the continuum phase. Solving Eq. (6) for a set of approximately energy-independent MQDT parameters, R'_{ij} and δ_j, yields τ^ϵ as a function of energy. Combining this relation with the energy normalization condition, $A_3^{\epsilon 2}=1$, the spectral amplitudes A_1^ϵ and A_2^ϵ can be determined.

Assuming there is no direct excitation of the continuum, the coefficient $c^\epsilon(t)$ long after the laser pulse can be written

$$c^\epsilon(\infty)=-i\mu^\epsilon\int_{-\infty}^{+\infty}F(t')e^{-i\omega t'}dt', \tag{7}$$

where

$$\mu^\epsilon=D_1A_1^\epsilon\cos\pi\nu_1'^\epsilon+D_2A_2^\epsilon\cos\pi\nu_2'^\epsilon, \tag{8}$$

$F(t)$ is the oscillating electric field of a single laser pulse with frequency $\omega=\epsilon-\epsilon_0$, and ϵ_0 is the energy of the intermediate $5d6p$ state. D_j represents the energy-independent parts of the dipole moments that connect the intermediate state to the bound channels $\phi_j^\epsilon(\mathbf{r})$. The energy-dependent parts of the dipole moments are given by the cosine terms in Eq. (7b), describing the variation of the dipole amplitude with the radial phase of the channel wave function.

The frequency spectrum of the excited wave packet is given by the cross section

$$\sigma^\epsilon=4\pi^2\alpha\omega|c^\epsilon|^2=4\pi^2\alpha\omega\mu^2|F^\epsilon|^2, \tag{9}$$

where α is the fine-structure constant. The variation in the autoionization yield as a function of the time delay between two identical laser pulses is related to the Fourier transform of the cross section σ^ϵ [16]:

$$S(\tau)=\left|\int_{-\infty}^{+\infty}\sigma^\epsilon e^{-i\epsilon\tau}d\epsilon\right|. \tag{10}$$

The rms interferogram $S(\tau)$ in Eq. (9) depends on the frequency *spectrum* of the laser pulse, not its temporal profile [16]. Therefore to reproduce the experimental data of Fig. 2(a) we need only know the MQDT coefficients R'_{ij} and δ_j, the dipole moments D_j, and the experimentally measured laser spectrum (see Sec. II).

IV. RESULTS

Rather than performing a seven-parameter fit of $S(\tau)$ to our experimental data in Fig. 2(a), we have used five MQDT parameters obtained from autoionization linewidth measurements by Neukammer *et al.* in a high-resolution cw laser experiment, $R'_{12}=-0.230$, $R'_{13}=-0.170$, $R'_{23}=-0.139$, $\delta_1=0.435$, and $\delta_2=0.485$ [17]. This leaves only the ratio of the dipole moments D_1/D_2 and an overall normalization constant to be adjusted to fit the experimental interferogram.

We calculated the excitation cross section σ^ϵ from Eq. (8) in the energy range of interest; i.e., from 4290 cm^{-1} to 4840 cm^{-1}, on a grid with 0.1-cm^{-1} energy spacing for various values of D_1/D_2. The best agreement between $S(\tau)$ and the experimental data is obtained for $D_2=0.4D_1$, and this result is shown in Fig. 2(b). Except for small discrepancies between $t=3$ and $t=4$ ps the overall agreement is good, particularly during the first 2 ps. The corresponding cross section is shown in Fig. 1(b). We also numerically solved an eight-dimensional eigenvalue equation similar to Eq. (6) using phase-shifted MQDT parameters from Ref. [18] to reproduce a $J=2$ excitation spectrum, but we found no improvement in the fit to the interferogram by including any $J=2$ channels.

The radial wave functions u_j^ϵ are not used explicitly in the interferogram calculation. Rather, the atomic structure has been incorporated implicitly in the energy-independent parts of the dipole moments D_j. However, to actually view the evolution of the Rydberg wave packet, we need explicit expressions for the radial wave functions. The u_j^ϵ are calculated by numerically integrating the one-electron Schrödinger equation using a Numerov algorithm [19]. Since the bound channels are embedded in the continuum the radial wave functions are energy normalized by requiring $\int u_j^{\epsilon 2}dr=\nu_j^{\epsilon 3}$ for $j=1,2$. We then calculate the wave packet's spatial distribution and temporal evolution by evaluating Eqs. (1)–(5). The explicit time dependence of the laser field F is ignored, but the temporal resolution is determined implicitly by the frequency bandwidth of the laser pulse.

Figures 3 and 4 summarize the theoretical results. Figure 3 shows the probabilities $P_1(t)$ and $P_2(t)$ for finding the wave packet in the bound $5d_{5/2}$ and $5d_{3/2}$ channels, respectively, and the total probability for being in a bound channel $[P_1(t)+P_2(t)=1-P_3(t)]$. Figures 4(a) and 4(c) show density plots of the spatial distribution and temporal evolution of the bound $5d_{5/2}$ and $5d_{3/2}$ wave packets. Figure 4(b) shows a density plot of the time-dependent $6s_{1/2}$ continuum electron density near $r=0$, which is a measure of the instantaneous autoionization rate.

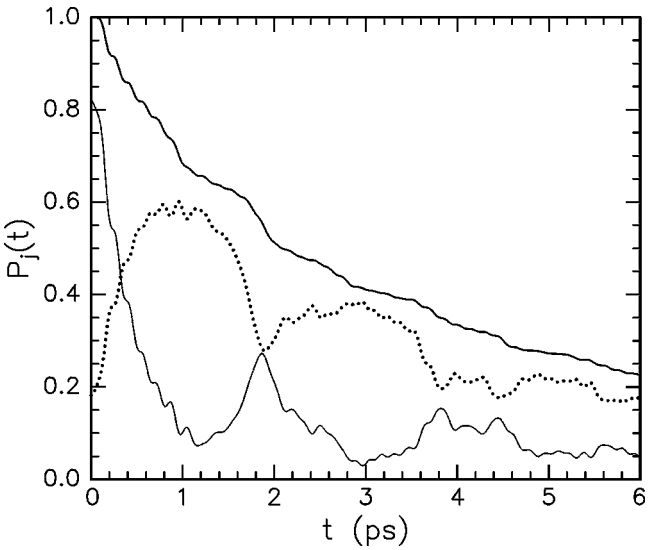

FIG. 3. Probabilities $P_j(t)$ for finding the wave packet in the $5d_{5/2}$ channel (thin solid curve), in the $5d_{3/2}$ channel (dotted curve), and their sum (thick solid curve), calculated using Eq. (5). The Kepler periods for the $5dn_{5/2}nd$, the low-n $5d_{3/2}nd$, and the high-n $5d_{3/2}nd$ wave packets are 0.16 ps, 0.95 ps, and 2.5 ps, respectively.

V. DISCUSSION

Of course it is not spectacularly surprising that even the very complex experimental interferogram in Fig. 2(a) can be reproduced by Eq. (9) since MQDT is known to reproduce frequency spectra of two-electron system very well [20]. However, since the experimental data are adequately described within the framework of MQDT, we are confident that numerical simulation gives an accurate representation of the spatial distribution and temporal evolution of the autoionizing radial wave packet. As a result, we can use the simulation pictures to obtain a better understanding of channel interactions in the time domain. Furthermore, because only two bound and one continuum $J=0$ channels are needed in the MQDT analysis, we can describe the complex evolution of the autoionizing wave packet using the relatively simple physical picture provided below.

During the laser excitation at $t=0$, a radial Rydberg wave packet is formed that is localized near the nucleus predominantly in the $5d_{5/2}$ channel, as is clearly seen in Fig. 3. Greater than 80% of the wave-packet probability resides in the $5d_{5/2}12d_{5/2}$ and $5d_{5/2}13d_{5/2}$ Rydberg levels. The packet has an average effective principal quantum number $\overline{n}^*=10$ and oscillates with a 160-fs Kepler period ($\tau_K=2\pi\overline{n}^{*3}$). When the Rydberg electron passes the $Ba^+5d_{5/2}$ core during each radial oscillation, a fraction of the probability amplitude scatters into the $5d_{3/2}$ bound channel (33% probability) or into the $6s_{1/2}$ continuum channel (7% probability). Every time the $5d_{5/2}$ wave packet returns to the core its population decreases. After seven Kepler periods ($\approx$1.1 ps) the $5d_{5/2}$ channel is almost completely depleted. While a nonnegligible amount of population has been lost to autoionization, most of the $5d_{5/2}$ amplitude has been ''shelved'' in the $5d_{3/2}$ configuration.

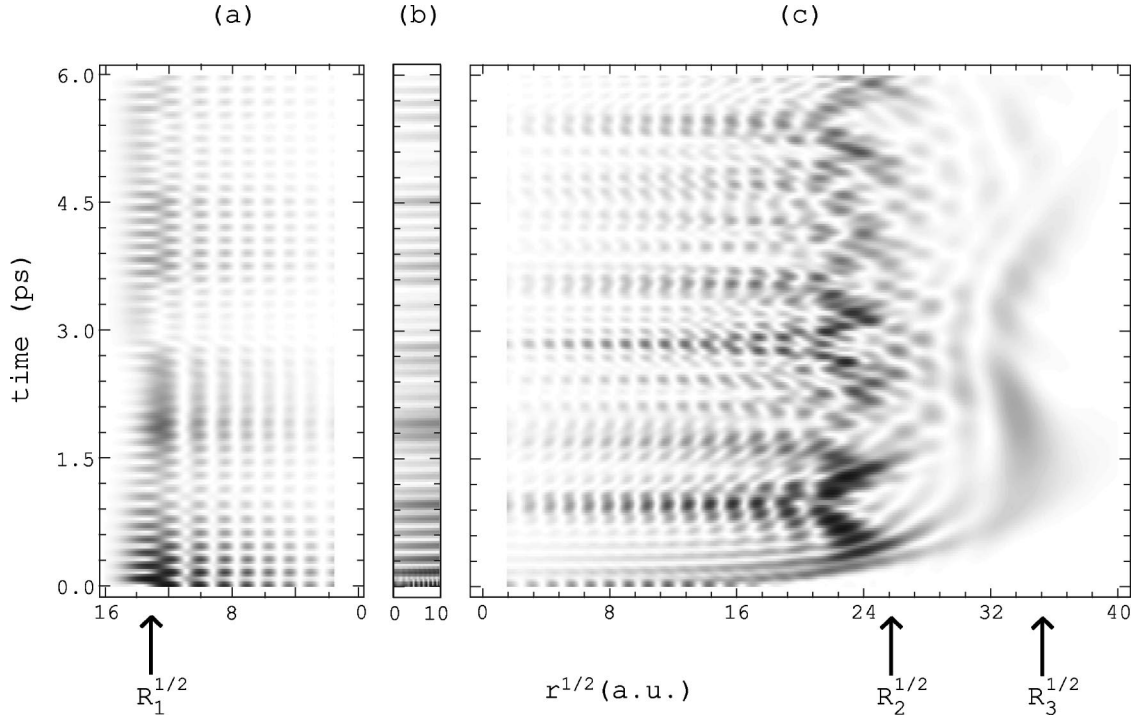

FIG. 4. Density plots of the probabilities $P_j(r,t)$ for finding the wave packet in (a) the bound $5d_{5/2}$ channel, (b) the continuum $6s_{1/2}$ channel, and (c) the bound $5d_{3/2}$ channel, calculated using Eq. (4). Note that the density plots are linear in time but that the spatial coordinate is the square root of the radial position r. The density plots clearly show three distinct wave packets with very different outer turning points R_1, R_2, and R_3. The gray scale is linear in intensity and dark (light) shading corresponds to a high (low) probability.

When population is transferred to the $5d_{3/2}$ channel only $5d_{3/2}nd_{3/2}$ states in the vicinity of the $5d_{5/2}12d_{5/2}$ and $5d_{5/2}13d_{5/2}$ levels are likely to be excited [see Fig. 1(b)]. As a result, two distinct $5d_{3/2}nd$ radial wave packets are formed with average effective principal quantum numbers $\overline{n}^* \approx 18.5$ and $\overline{n}^* \approx 25.5$. These packets orbit the Ba^+ core with much longer Kepler periods, $\tau_K \approx 0.95$ ps and $\tau_K \approx 2.5$ ps, respectively. When the Rydberg population ''shelved'' in these wave packets returns to the $Ba^+(5d_{3/2})$ core, population can scatter into the $6s_{1/2}$ continuum or back into the $5d_{5/2}$ bound configuration. The $5d_{3/2}$ population ''shelving'' is equivalent to autoionization into a discrete quasicontinuum. Unlike autoionization into a flat continuum, population in the $5d_{3/2}nd$ wave packets eventually returns to the ion core where rescattering into the $5d_{5/2}n'd$ configurations is likely.

Rydberg population that was shelved in the low-n part of the $5d_{3/2}$ channel first returns to the core after 1 ps. However, due to interferences between the $5d_{3/2}$ and $5d_{5/2}$ channels during this return, little net transfer between these two bound configurations occurs. In contrast, nearly all of the population that is shelved in the low-n $5d_{3/2}$ wave packet rescatters into the $5d_{5/2}$ channel during its second return to the ion core near $t=1.9$ ps. Nevertheless, inspection of Fig. 3 indicates that only 50% of the total bound character resides in the $5d_{5/2}$ configuration at $t=1.9$ ps. The other 50% remains shelved in the high-n $5d_{3/2}$ wave packet, which does not to return to the core for another 0.6 ps.

Scattering between the bound channels continues, but with decreasing amplitude due to autoionization losses. Although the discussion thus far has concentrated on bound-bound coupling, scattering into the unbound $6s_{1/2}$ continuum also occurs every time the Rydberg electron passes near the $5d_j$ ion core. The slope of the bound-state population curve (the thick line in Fig. 3) is equal to the negative of the autoionization rate. Inspection of the total population curve indicates that autoionization occurs in bursts as the wave packets pass the nucleus. The instantaneous autoionization rate is also proportional to the probability of finding both electrons near the ion core in the $6s_{1/2}$ continuum configuration [see Fig. 4(b)].

Further insight into the wave-packet dynamics is gained by looking directly at the probability distributions in the three $J=0$ configurations. Figure 4(a) shows a density plot of the time-dependent $5d_{5/2}$ probability distribution. The analogous distribution for the $5d_{3/2}$ configuration is shown in Fig. 4(c). Initially, the ion core is likely to be found in the $5d_{5/2}$ configuration, with the Rydberg electron close to the nucleus $r=0-250a_0$. In only 80 fs ($0.5\tau_K$) the Rydberg electron is localized near its classical outer turning point at $R_1=175a_0$. It returns to the ion core after 160 fs. As one would expect for a two-state wave packet, the radial oscillations remain strong during the entire time the wave packet is monitored, except near $t=2$ ps. In fact, between $t=1.8$ and $t=2.4$ ps the $5d_{5/2}$ part of the total wave function shows no temporal evolution at all and strongly resembles the stationary $5d_{5/2}12d$ wave function. During this time interval, the $5d_{5/2}$ channel, which was almost completely depleted at $t=1$ ps, has been repopulated through rescattering from the low-n $5d_{3/2}$ wave packet. However, the low-n part of the $5d_{3/2}$ population is composed entirely of $5d_{3/2}nd$ states *in the vicinity of the* $5d_{5/2}12d$ *level*. The dynamic $5d_{5/2}nd$ wave packet is not reconstructed until the high-n $5d_{3/2}$ wave packet returns to the core after 2.5 ps. The absence of any spatial modulation in the $5d_{5/2}$ wave function results in the small modulation depth of the rms signal for 1.6 ps$<t<$2.4 ps in Fig. 2. Because the $5d_{5/2}$ part of the wave function does not move, there is essentially no change in the overlap between the initial wave packet and its configuration during this time interval. It is interesting that the two-electron dynamics conspire to create a quasi-$5d_{5/2}$ eigenstate from the laser-excited two-state wave packet.

Turning to Fig. 4(c), it is clear that at $t=0$ approximately 20% of the excited-state population travels away from the nucleus in a $5d_{3/2}$ radial wave packet. Every time the $5d_{5/2}$ packet passes the core (i.e., every 160 fs) probability amplitude scatters into the $5d_{3/2}$ channel, launching additional long-range wave packets. The interaction between the two valence electrons results in kinetic-energy exchange and a spin-flip of both electrons. Because the Rydberg electron has greater kinetic energy in the new spin-orbit potential, it moves much further away from the Ba^+ core. When the $5d_{3/2}$ wave packet reaches $R_2=680a_0$, it splits into two parts: one that reverses its direction and begins traveling inwards with a Kepler period of 0.95 ps, and another that continues to move away from the nucleus until it reaches an outer turning point at $R_3=1300a_0$ and returns to the core after a corresponding Kepler period of 2.5 ps.

It is interesting that the spatial separation of the high-n and low-n $5d_{3/2}$ wave packets removes the 160-fs spatiotemporal modulation in the $5d_{3/2}$ probability distribution. Recall that this rapid modulation is produced by the periodic dumping of population into the $5d_{3/2}$ channel by the oscillating $5d_{5/2}$ wave packet. The rapid 160-fs beating is characteristic of two interfering waves with different energies, and only occurs if the two $5d_{3/2}$ packets overlap in space.

VI. CONCLUSION

We have studied the dynamics of radial Rydberg wave packets in an autoionizing two-electron system. We observed temporal oscillation of population between two, strongly coupled, bound Rydberg *series* embedded in a continuum. The complex evolution of the autoionizing wave packet was probed by bound-state interferometry and was well described by three-channel quantum-defect theory, enabling us to calculate the temporal evolution and spatial distribution of the wave packet in each of the three dielectronic configurations. Observations include the coherent beating of three distinct radial Rydberg wave packets, the shelving of population in long-lived states, and the creation of quasi-eigenstates through electron scattering within the laser-excited two-electron wave packets.

ACKNOWLEDGMENTS

We gratefully acknowledge stimulating discussions with T.F. Gallagher and the financial support of the NSF, the UVA AEP, and the Packard Foundation.

[1] J.A. Yeazell and C.R. Stroud, Phys. Rev. Lett. **60**, 1494 (1988); A. ten Wolde, L.D. Noordam, A. Lagendijk, and H.B. van Linden van den Heuvell, *ibid.* **61**, 2099 (1988).
[2] W.A. Henle, H. Ritsch, and P. Zoller, Phys. Rev. A **36**, 683 (1987).
[3] F. Robichaux and W.T. Hill III, Phys. Rev. A **54**, 3276 (1996); L.G. Hanson and P. Lambropoulos, Phys. Rev. Lett. **74**, 5009 (1995).
[4] D.W. Schumacher, D.I. Duncan, R.R. Jones, and T.F. Gallagher, J. Phys. B **29**, L397 (1996); D.W. Schumacher, B.J. Lyons, and T.F. Gallagher, Phys. Rev. Lett. **78**, 4359 (1997).
[5] M.B. Campbell, T.J. Bensky, and R.R. Jones, Phys. Rev. A **57**, 4616 (1998).
[6] J.E. Thoma and R.R. Jones, Phys. Rev. Lett. **83**, 516 (1999); J.B.M. Warntjes, C. Wesdorp, F. Robicheaux, and L.D. Noordam, *ibid.* **83**, 512 (1999).
[7] R. van Leeuwen, M.L. Bajema, and R.R. Jones, Phys. Rev. Lett. **82**, 2852 (1999).
[8] X. Chen and J.A. Yeazell, Phys. Rev. Lett. **81**, 5772 (1998).
[9] W.S. Warren, H. Rabitz, and M. Dahleh, Science **259**, 1581 (1993), and references therein.
[10] X. Wang and W.E. Cooke, Phys. Rev. Lett. **67**, 976 (1991); X. Wang and W.E. Cooke, Phys. Rev. A **46**, 4347 (1992).
[11] W.E. Cooke, T.F. Gallagher, S.A. Edelstein, and R.M. Hill, Phys. Rev. Lett. **40**, 178 (1978).
[12] N.F. Sherer *et al.*, Chem. Phys. **93**, 856 (1990); L.D. Noordam, D.I. Duncan, and T.F. Gallagher, Phys. Rev. A **45**, 4734 (1992); R.R. Jones, C.S. Raman, D.W. Schumacher, and P.H. Bucksbaum, Phys. Rev. Lett. **71**, 2575 (1993).
[13] U. Fano, Phys. Rev. A **2**, 353 (1970); M.J. Seaton, Rep. Prog. Phys. **46**, 167 (1983).
[14] W.E. Cooke and C.L. Cromer, Phys. Rev. A **32**, 2725 (1985).
[15] C.E. Moore, *Atomic Energy Levels*, Natl. Bur. Stand. Ref. Data, Natl. Bur. Stand. (U.S.) (U.S. GPO, Washington, DC, 1971), Vol. II.
[16] R.R. Jones, D.W. Schumacher, T.F. Gallagher, and P.H. Bucksbaum, J. Phys. B **28**, L405 (1995).
[17] J. Neukammer, H. Rinneberg, G. Jönsson, W.E. Cooke, H. Hieronymus, A. König, and K. Vietzke, Phys. Rev. Lett. **55**, 1979 (1985).
[18] E. Bente and W. Hogervorst, Z. Phys. D **14**, 119 (1989).
[19] M.L. Zimmermann, M.G. Littman, M.M. Kash, and D. Kleppner, Phys. Rev. A **20**, 2251 (1979).
[20] T.F. Gallagher, *Rydberg Atoms*, 1st ed. (Cambridge University Press, Cambridge, 1994).